Technical report from Automatic Control at Linköpings universitet

Road Geometry Estimation and Vehicle Tracking using a Single Track Model

Christian Lundquist, Thomas B. Schön

Division of Automatic Control

E-mail: lundquist@isy.liu.se, schon@isy.liu.se

3rd March 2008

Report no.: LiTH-ISY-R-2844
Accepted for publication in IEEE Intelligent Vehicles Symposium, Eindhoven, the Netherlands, June 4-6, 2008

Address:
Department of Electrical Engineering
Linköpings universitet
SE-581 83 Linköping, Sweden

WWW: http://www.control.isy.liu.se

AUTOMATIC CONTROL
REGLERTEKNIK
LINKÖPINGS UNIVERSITET

Abstract

This paper is concerned with the, by now rather well studied, problem of integrated road geometry estimation and vehicle tracking. The main differences to the existing approaches are that we make use of an improved host vehicle model and a new dynamic model for the road. The problem is posed within a standard sensor fusion framework, allowing us to make good use of the available sensor information. The performance of the solution is evaluated using measurements from real and relevant traffic environments from public roads in Sweden.

Keywords: road geometry, vehicle tracking, sensor fusion, Kalman filter, single track model

Road Geometry Estimation and Vehicle Tracking using a Single Track Model

Christian Lundquist, Thomas B. Schön

2008-03-03

Abstract

This paper is concerned with the, by now rather well studied, problem of integrated road geometry estimation and vehicle tracking. The main differences to the existing approaches are that we make use of an improved host vehicle model and a new dynamic model for the road. The problem is posed within a standard sensor fusion framework, allowing us to make good use of the available sensor information. The performance of the solution is evaluated using measurements from real and relevant traffic environments from public roads in Sweden.

Contents

1 Introduction

We are concerned with the, by now rather well studied, problem of automotive sensor fusion. More specifically, we consider the problem of integrated road geometry estimation and vehicle tracking making use of an improved host vehicle model. The overall aim in the present paper is to extend the existing results to a more complete treatment of the problem by making better use of the available information.

In order to facilitate a systematic treatment of this problem we need dynamical models for the host vehicle, the road and the leading vehicles. These models are by now rather well understood. However, in studying sensor fusion problems this information tends not to be used as much as it could. Dynamic vehicle modelling is a research field in itself and a solid treatment can be found in for example [16, 14]. The leading vehicles can be successfully modelled using the geometrical constraints and their derivatives w.r.t. time. Finally, dynamic models describing the road are rather well treated, see e.g., [6, 5, 4]. The resulting state-space model, including host vehicle, road and leading vehicles, can then be written in the form

$$x_{t+1} = f(x_t, u_t) + w_t, \tag{1a}$$

$$y_t = h(x_t, u_t) + e_t, \tag{1b}$$

where x_t denotes the state vector, u_t denotes the input signal, w_t denotes the process noise, y_t denotes the measurements and e_t denotes the measurement noise. Once we have derived a model in the form (1) the problem has been transformed into a standard nonlinear estimation problem. This problem has been extensively studied within the control and the target tracking communities for many different application areas and there are many different ways to solve it, including the popular Extended Kalman Filter (EKF), the particle filter and the Unscented Kalman Filter (UKF), see e.g., [1, 13] for more information on this topic.

As mentioned above, the problem studied in this paper is by no means new, see e.g., [5, 4] for some early work without using the motion of the leading vehicles. These papers are still very interesting reading and contain much of the underlying ideas that are being used today. It is also interesting to note that the importance of sensor fusion was stressed already in these early papers. The next step in the development was to introduce a radar sensor as well. The idea was that the motion of the leading vehicles reveals information about the road geometry [21, 9, 10]. Hence, if the leading vehicles can be accurately tracked, their motion can be used to improve the road geometry estimates, computed using only information about the host vehicle motion and information about the road inferred from a vision sensor. This idea has been further refined and developed in [8, 19, 6]. However, the dynamic model describing the host vehicle used in all of these later works were significantly simplified as compared to the one used in [5, 4, 3]. It consists of 2 states, the distance from the host vehicle to the white lane and the heading (yaw) angle of the host vehicle. Hence, it does not contain any information about the host vehicles velocity vector. Information of this kind is included in the host vehicle model employed in the present paper.

The main contribution of this work is to pose and solve a sensor fusion problem that makes use of the information from all the available sensors. This

is achieved by unifying all the ideas in the above referenced papers. The host vehicle is modelled in more detail, it bears most similarity to the model used in [5, 4]. Furthermore, we include the motion of the leading vehicles, using the idea introduced in [21]. The resulting sensor fusion problem provides a rather systematic treatment of the information from the sensors measuring the host vehicle motion (inertial sensors, steering wheel sensors and wheel speed sensors) and the sensors measuring the vehicle surroundings (vision and radar).

We will show how the suggested sensor fusion approach performs in practice, by evaluating it using measurements from real and relevant traffic environments from public roads in Sweden.

2 Dynamic Models

In this section we will derive the differential equations describing the motion of the host vehicle (Section 2.2), the road (Section 2.3) and the leading vehicles (Section 2.4), also referred to as targets. However, before we embark on deriving these equations we introduce the overall geometry and some notation in Section 2.1.

2.1 Geometry and Notation

The coordinate frames describing the host vehicle and one leading vehicle are defined in Figure 1. The inertial reference frame is denoted by R and its origin is

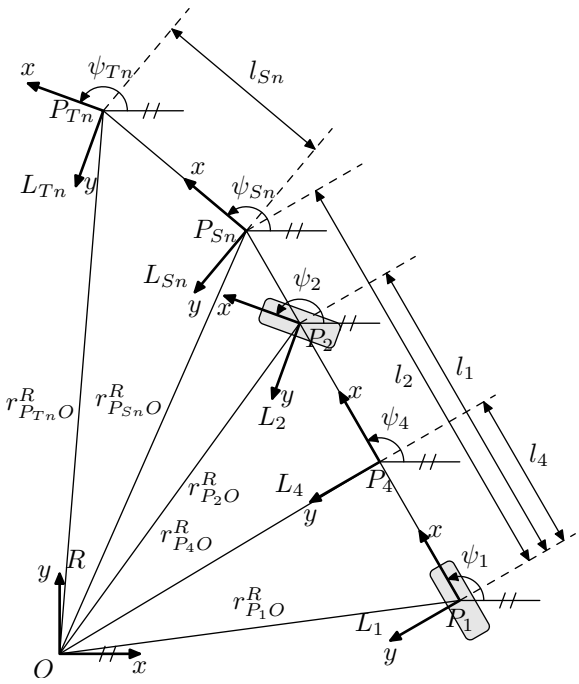

Figure 1: Coordinate frames describing the host vehicle and one leading vehicle Tn.

O, the other frames are denoted by L_i, with origin in P_i. P_1 and P_2 are attached to the rear and front wheel axle of the host vehicle, respectively. P_3 is used to describe the road and P_4 is located in the center of gravity (CoG) for the host vehicle. Furthermore, L_{Sn} is associated to the observed leading vehicle n, with P_{Sn} at the sensor of the host vehicle. Finally, L_{Tn} is also associated with the observed leading vehicle n, but its origin P_{Tn} is located at the leading vehicle. Velocities are defined as the movement of a frame L_i relative to the inertial reference frame R, but typically resolved in the frame L_i, for example $v_x^{L_4}$ is the velocity of the L_4 frame in its x-direction. The same convention holds for the acceleration $a_x^{L_4}$. In order to simplify the notation we leave out L_4 when referring to the host vehicle's longitudinal velocity v_x. This notation will be used when referring to the various coordinate frames. However, certain frequently used quantities will be renamed, in the interest of readability. The measurements are denoted by using subscript m or a completely different notation. Furthermore, the notation used for the rigid body dynamics is in accordance with [12].

2.2 Host Vehicle

We will only be concerned with the host vehicle motion during normal driving situations and not at the wheel-track adhesion limit. This implies that the single track model [16] is sufficient for the present purposes. This model is also referred to to as the bicycle model. The geometry of the single track model with slip angles is shown in Figure 2. It is here worth to point out that the velocity vector of the host vehicle is typically not in the same direction as the longitudinal axis of the host vehicle. Instead the vehicle will move along a path at an angle β with the longitudinal direction of the vehicle if the slip angles are considered. This angle β is referred to as the float angle [17] or vehicle body side slip angle [14]. Lateral slip is an effect of cornering. To turn, a vehicle needs to be affected by lateral forces. These are provided by the friction when the wheels slip.

The slip angle α_i is defined as the angle between the central axis of the wheel and the path along which the wheel moves. The phenomenon of side slip is mainly due to the lateral elasticity of the tire. For reasonably small slip angles, at maximum 3 deg, it is a good approximation to assume that the lateral friction force of the tire F_i is proportional to the slip angle,

$$F_i = C_{\alpha i}\alpha_i. \tag{2}$$

The parameter $C_{\alpha i}$ is called cornering stiffness and describes the cornering behaviour of the tire. A deeper analysis of slip angles can be found in e.g., [16].

2.2.1 Geometric Constraints

From Figure 1 we have the geometric constraints:

$$r_{P_1O}^R + A^{RL_1} \cdot r_{P_2P_1}^{L_1} - r_{P_2O}^R = 0. \tag{3}$$

In this document we will use the the planar coordinate transformation matrix

$$A^{RL_i} = \begin{pmatrix} \cos\psi_i & -\sin\psi_i \\ \sin\psi_i & \cos\psi_i \end{pmatrix} \tag{4}$$

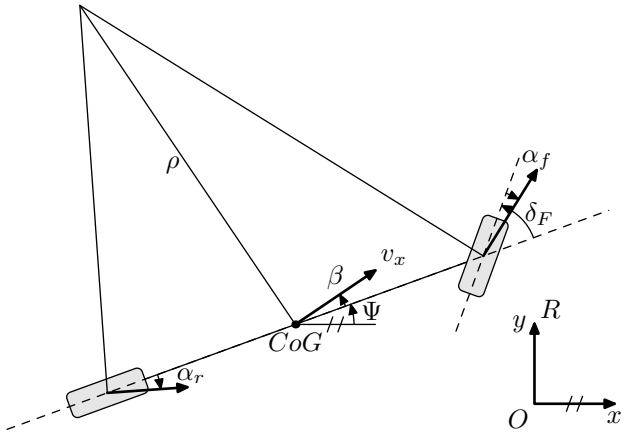

Figure 2: Illustration of the geometry for the single track model, describing the motion of the host vehicle. The host vehicle velocity vector v_x is defined from the CoG and its angle to the longitudinal axis of the vehicle is denoted by β, referred to as the float angle or vehicle body side slip angle. Furthermore, the slip angles are referred to as α_f and α_r. The front wheel angle is denoted by δ_F and the current radius is denoted by ρ.

to map a vector, represented in L_i, into a vector, represented in R, where ψ_i is the angle of rotation from R to L_i. The geometric displacement vector $r^R_{P_1O}$ is the direct straight line from O to P represented with respect to the frame R. In our case

$$r^{L_1}_{P_2P_1} = \begin{pmatrix} l_1 \\ 0 \end{pmatrix} \tag{5}$$

yields

$$x^R_{P_2O} = l_1 \cos\psi_1 + x^R_{P_1O}, \tag{6a}$$
$$y^R_{P_2O} = l_1 \sin\psi_1 + y^R_{P_1O}. \tag{6b}$$

For the coordinates of the car center of gravity $(x^R_{P_4O}, y^R_{P_4O})$ it holds that

$$x^R_{P_4O} - l_4 \cos\psi_1 - x^R_{P_1O} = 0, \tag{7a}$$
$$y^R_{P_4O} - l_4 \sin\psi_1 - y^R_{P_1O} = 0, \tag{7b}$$

where l_4 is the distance between the center of gravity and the rear wheel axle, compare with Figure 1.

Furthermore, the front wheel angle δ_F, i.e. the angle between the longitudinal direction of the front wheel and the longitudinal axis of the host vehicle, is defined as

$$\delta_F \triangleq \psi_2 - \psi_1. \tag{8}$$

2.2.2 Kinematic Constraints

The velocity is measured at the rear axis by taking the mean value of two rear wheels speed. Besides the easier calculations, another advantage of just using

the rear wheel speeds is that they have less longitudinal slip due to the front wheel traction of a modern Volvo.[1] The host vehicles velocity can be expressed as

$$A^{L_1 R} \cdot \dot{r}^R_{P_1 O} = \begin{pmatrix} v_x^{L_1} \\ v_y^{L_1} \end{pmatrix}, \tag{9}$$

which can be rewritten as

$$\dot{x}^R_{P_1 O} \cos\psi_1 + \dot{y}^R_{P_1 O} \sin\psi_1 = v_x^{L_1}, \tag{10a}$$

$$-\dot{x}^R_{P_1 O} \sin\psi_1 + \dot{y}^R_{P_1 O} \cos\psi_1 = v_y^{L_1}. \tag{10b}$$

Using (6) and the new definitions of $v_x^{L_1}$ (10a) and $v_y^{L_1}$ (10b) we get

$$\dot{\psi}_1 = \frac{v_x^{L_1}}{l_1} \tan(\delta_F - \alpha_f) - \frac{v_y^{L_1}}{l_1}, \tag{11a}$$

$$v_y^{L_1} = -v_x^{L_1} \tan\alpha_r. \tag{11b}$$

having in mind that the velocities $v_x^{L_1}$ and $v_y^{L_1}$ have their origin in the host vehicle's rear axle. In order to simplify the notation we also define the velocities in the vehicle's center of gravity as $v_x^{L_4} = v_x^{L_1} = v_x$ and $v_y^{L_4} = v_y^{L_1} + \dot{\psi}_1 \cdot l_4$. The host vehicles float angle β is defined as,

$$\tan\beta = \frac{v_y^{L_4}}{v_x}, \tag{12}$$

and inserting this relation in (11) yields us

$$\tan\alpha_r = -\tan\beta + \frac{\dot{\psi}_1 \cdot l_4}{x_v}, \tag{13}$$

$$\tan(\delta_F - \alpha_f) = \frac{\dot{\psi}_1 \cdot (l_1 - l_4)}{v_x} + \tan\beta. \tag{14}$$

Under normal driving conditions we can assuming small α and β angles ($\tan\alpha = \alpha$ and $\tan\beta = \beta$ respectively), thus:

$$\alpha_r = -\beta + \frac{\dot{\psi}_1 \cdot l_4}{x_v}, \tag{15a}$$

$$\alpha_f = -\frac{\dot{\psi}_1 \cdot (l_1 - l_4)}{v_x} - \beta + \tan\delta_F, \tag{15b}$$

holds.

2.2.3 Motion Model

Following this introduction to the host vehicle geometry and its kinematic constraints we are now ready to give an expression of the host vehicle's velocity vector, resolved in the inertial frame R,

$$\dot{x}^R_{P_4 O} = v_x \cos(\psi_1 + \beta), \tag{16a}$$

$$\dot{y}^R_{P_4 O} = v_x \sin(\psi_1 + \beta), \tag{16b}$$

[1] This project was carried out together with Volvo Car Corporation and the Intelligent Vehicle Safety System Program (IVSS). The results were validated using a Volvo S80.

which is governed by the yaw angle ψ_1 and the float angle β. Hence, in order to find the state-space model we are looking for, we need the differential equations describing the evolution of these angles over time. Differentiating (7) we obtain the corresponding relation for the accelerations:

$$\ddot{x}^R_{P_4O} + l_4\ddot{\psi}_1 \sin\psi_1 + l_4\dot{\psi}_1^2 \cos\psi_1 - \ddot{x}^R_{P_1O} = 0, \tag{17}$$

$$\ddot{y}^R_{P_4O} - l_4\ddot{\psi}_1 \cos\psi_1 + l_4\dot{\psi}_1^2 \sin\psi_1 - \ddot{y}^R_{P_1O} = 0. \tag{18}$$

Substituting the expressions of the host vehicle's accelerations yields

$$a_x^{L_4} \cos\psi_1 - a_y^{L_4} \sin\psi_1 + l_4\ddot{\psi}_1 \sin\psi_1 + l_4\dot{\psi}_1^2 \cos\psi_1 - a_x^{L_1} \cos\psi_1 - a_y^{L_1} \sin\psi_1 = 0 \tag{19}$$

and

$$a_x^{L_4} \sin\psi_1 + a_y^{L_4} \cos\psi_1 - l_4\ddot{\psi}_1 \cos\psi_1 + l_4\dot{\psi}_1^2 \sin\psi_1 - a_x^{L_1} \sin\psi_1 + a_y^{L_1} \cos\psi_1 = 0. \tag{20}$$

By combining the two equations and separating the variables in front of the sinus and cosine we get:

$$a_y^{L_4} = a_y^{L_1} + l_4\ddot{\psi}_1.$$

For the centers of gravity, we can use Newton's second law of motion, $F = ma$. We only have to consider the lateral axis (y), since longitudinal movement is a measured input. This gives us

$$\sum F_i = m\, a_y^{L_4}, \tag{21}$$

where

$$a_y^{L_4} = \dot{v}_y^{L_4} + \dot{\psi}_1\, v_x, \tag{22}$$

and

$$\dot{v}_y^{L_4} = \frac{d}{dt}(\beta v_x) = v_x\dot{\beta} + \dot{v}_x\beta, \tag{23}$$

holds for small angles. The external forces are in this case the slip forces from the wheels, compare with (2). Merging these expressions into Newton's law, we have

$$C_{\alpha f}\, \alpha_f \cos\delta_F + C_{\alpha r}\, \alpha_r = m(v_x\dot{\psi} + v_x\dot{\beta} + \dot{v}_x\beta), \tag{24}$$

where m denotes the mass of the host vehicle. In the same manner Euler's equation

$$\sum M_i = J\, \ddot{\psi}_1 \tag{25}$$

is used to obtain the relations for the angular accelerations

$$(l_2 - l_4)\, C_{\alpha f}\, \alpha_f \cos\delta_F - l_4\, C_{\alpha r}\, \alpha_r = J\, \ddot{\psi}_1, \tag{26}$$

where J denotes the moment of inertia of the vehicle about its vertical axis in the center of gravity. By using the relations of the wheels' slip angle (15) in (24) and (26) we obtain

$$m(v_x\dot{\psi} + v_x\dot{\beta} + \dot{v}_x\beta) = = C_{\alpha f}\left(\frac{\dot{\psi}_1(l_1 - l_4)}{v_x} + \beta - \tan\delta_F\right)\cos\delta_F + C_{\alpha r}\left(\beta - \frac{\dot{\psi}_1 l_4}{v_x}\right) \tag{27}$$

and

$$J_1\ddot{\psi}_1 =$$
$$= (l_1 - l_4)\, C_{\alpha f} \left(\frac{\dot{\psi}_1 (l_1 - l_4)}{v_x} + \beta - \tan\delta_F \right) \cos\delta_F - l_4\, C_{\alpha r} \left(\beta - \frac{\dot{\psi}_1 l_4}{v_x} \right) \quad (28)$$

which can be rewritten as

$$\ddot{\psi}_1 = \beta \frac{(-(l_1 - l_4) C_{\alpha f} \cos\delta_F + l_4 C_{\alpha r})}{J} - \dot{\psi}_1 \frac{C_{\alpha f}(l_1 - l_4)^2 \cos\delta_F + C_{\alpha r} l_4^2}{J v_x} + \frac{(l_1 - l_4) C_{\alpha f} \tan\delta_F}{J}, \quad (29)$$

$$\dot{\beta} = \beta \frac{-C_{\alpha f} \cos\delta_F - C_{\alpha r} - \dot{v}_x m}{m v_x} - \dot{\psi}_1 \left(1 + \frac{C_{\alpha f}(l_1 - l_4)\cos\delta_F - C_{\alpha r} l_4}{v_x^2 m} \right) + \frac{C_{\alpha f} \sin\delta_F}{m v_x}, \quad (30)$$

These equations are well-known from the literature, see e.g., [14].

2.3 Road

The essential component in describing the road geometry is the curvature c, which is defined as the curvature of the white lane marking to the left of the host vehicle. An overall description of the road geometry is given in Figure 3. In order to model the road curvature we introduce the road coordinate frame L_3, with its origin P_3 on the white lane marking to the left of the host vehicle, with $x^{L_1}_{P_3 P_1} = l_2$. This implies that the frame L_3 is moving with the x-axis of the host vehicle. The angle of the L_3 frame ψ_3 is defined as the tangent of the road in $x^{L_3} = 0$, see Figure 4. This implies that ψ_3 is defined as

$$\psi_3 \triangleq \psi_1 + \delta_r, \quad (31)$$

where δ_r is the angle between the tangent of the road curvature and the longitudinal axis of the host vehicle, i.e.,

$$\delta_r = \beta + \delta_R. \quad (32)$$

Here, δ_R is the angle between the host vehicles direction of motion (velocity vector) and the road curvature tangent. Hence, inserting (32) into (31) we have

$$\psi_3 = \psi_1 + \beta + \delta_R. \quad (33)$$

Furthermore, the road curvature c is typically parameterized according to

$$c(x_c) = c_0 + c_1 x_c, \quad (34)$$

where x_c is the position along the road in a road aligned coordinate frame. Furthermore, c_0 describes the local curvature at the host vehicle position and c_1 is the distance derivative (hence, the rate of change) of c_0. It is common to

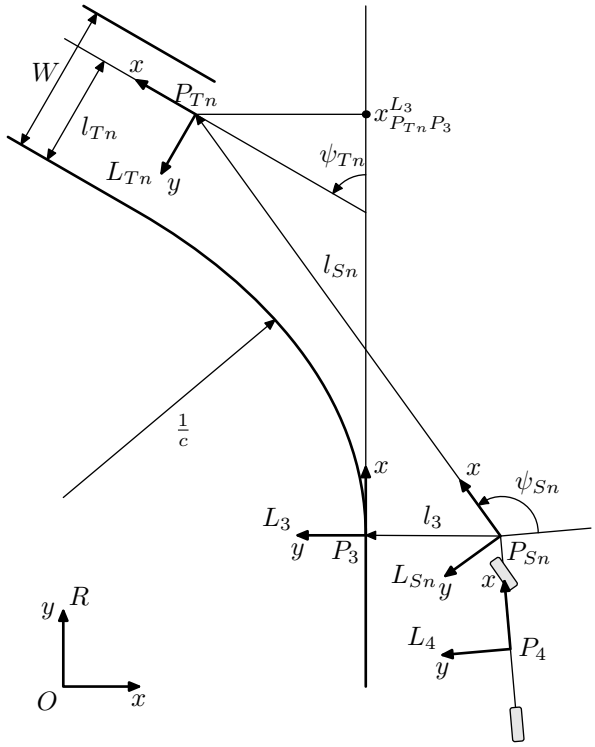

Figure 3: Relations between the leading vehicles Tn, the host vehicle and the road. The distance between the host vehicle path and the white lane to its left (where the road curvature is defined) is l_3. The lane width is W.

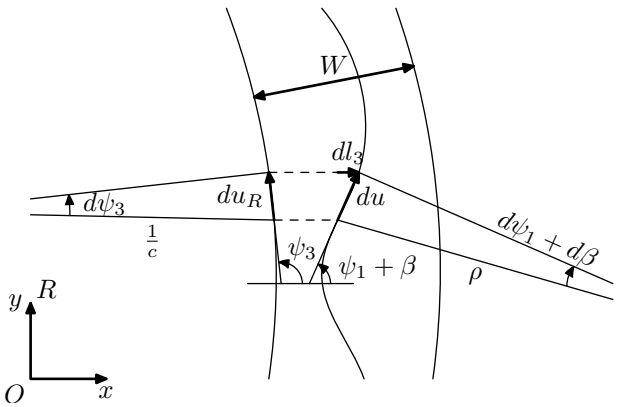

Figure 4: Representation of the road curvature c_0, the radius ρ of the (driven) path and the angles $\delta_R = \psi_3 - (\psi_1 + \beta)$. The lane width is W.

make use of a road aligned coordinate frame when deriving an estimator for the road geometry, a good overview of this approach is given in [6]. However, we will make use of a Cartesian coordinate frame. Since the road can be approximated by the first quadrant of an ellipse, the Pythagorean theorem can be used to

describe the position of the road in the L_3-system as

$$y^{L_3} = -\text{sign}(c)\left(\sqrt{\left(\frac{1}{c_0 + c_1 x^{L_3}}\right)^2 - (x^{L_3})^2} - \frac{1}{c_0}\right). \tag{35}$$

A good polynomial approximation of the shape of the road curvature is given by

$$y^{L_3} = \frac{c_0}{2}(x^{L_3})^2 + \frac{c_1}{6}(x^{L_3})^3, \tag{36}$$

see e.g., [4, 6]. The two expressions are compared in Figure 5, where the road curvature parameters are $c_0 = 0.002$ (500 m) and $c_1 = -10^{-7}$. The difference between the two curves is negligible, and due to its simplicity the polynomial approach in (36) will be used in the following derivations. Rewriting (36) with respect to the host vehicles coordinate frame yields

$$y^{L_4} = l_3 + x^{L_4}\tan\delta_r + \frac{c_0}{2}(x^{L_4})^2 + \frac{c_1}{6}(x^{L_4})^3, \tag{37}$$

where $l_3(t)$ is defined as the time dependent distance between the host vehicle and the lane to the left.

The following dynamic model is often used for the road

$$\dot{c}_0 = v_x c_1, \tag{38a}$$

$$\dot{c}_1 = 0, \tag{38b}$$

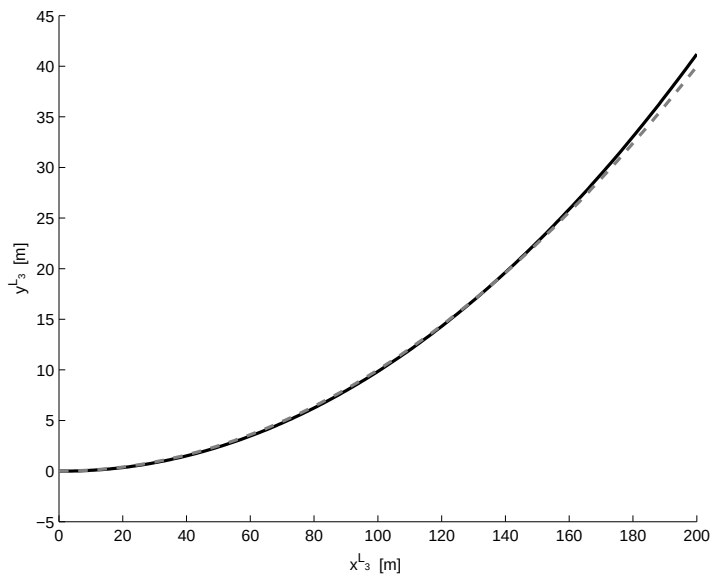

Figure 5: An example of the road curvature where the host vehicle is situated in $x = 0$ and its longitudinal direction is in the direction of the x-axis. The solid line is a plot of Equation (35) and the dashed line of (36) respectively. The road curvature parameters are $c_0 = 0.002$ (500 m) and $c_1 = -10^{-7}$ in this example.

which in discrete time can be interpreted as a velocity dependent integration of white noise. It is interesting to note that (38) reflects the way in which roads are commonly built [4]. However, we will now derive a new dynamic model for the road that makes use of the road geometry introduced above.

2.3.1 Road Angle

Assume that du_R is a part of the road curvature or an arc of the road circle with the angle $d\psi_3$, see Figure 4. A segment of the road circle can be described as

$$du_R = \frac{1}{c_0} \cdot d\psi_3, \tag{39}$$

which after division with the differential w.r.t. time dt is given by

$$\frac{du_R}{dt} = \frac{1}{c_0} \cdot \frac{d\psi_3}{dt}, \tag{40a}$$

$$v_x = \frac{1}{c_0} \cdot \dot{\psi}_3, \tag{40b}$$

where we have assumed that $\frac{du_R}{dt} = v_x \cos\delta_R \approx v_x$. Re-ordering the equation and using the derivative of (33) to substitute ψ_3 yields

$$\dot{\delta}_R = c_0 v_x - (\dot{\psi}_1 + \dot{\beta}). \tag{41}$$

A similar relation has been used in [4, 15].

2.3.2 Road Curvature

Differentiating (41) w.r.t. time gives

$$\ddot{\delta}_R = \dot{c}_0 v_x + c_0 \dot{v}_x - \ddot{\psi}_1 - \ddot{\beta}, \tag{42}$$

from which we have

$$\dot{c}_0 = \frac{\ddot{\delta}_R + \ddot{\psi}_1 + \ddot{\beta} - c_0 \dot{v}_x}{v_x}. \tag{43}$$

Assume $\ddot{\delta}_R = 0$, inserting $\ddot{\psi}_1$ which was given in (29), and differentiating $\dot{\beta}$, from (30), w.r.t. time yields

$$\begin{aligned}
\dot{c}_0 = \frac{1}{(Jm^2 v_x)^4} \Big(& C_{\alpha r}^2 (J + l_4^2 m)(-\dot{\psi}_1 l_4 + \beta v_x) \\
& + C_{\alpha f}^2 (J + (l_1 - l_4)^2 m)(\dot{\psi}_1 (l_1 - l_4) + (\beta - \delta_F) v_x) \\
& + C_{\alpha r} J m (-3\dot{\psi}_1 \dot{v}_x l_4 + 3\beta \dot{v}_x v_x + \dot{\psi}_1 v_x^2) \\
& + \dot{v}_x J m^2 v_x (2\beta \dot{v}_x + v_x (\dot{\psi}_1 - c_0 v_x)) \\
& + C_{\alpha f} (C_{\alpha r} (J + l_4(-l_1 + l_4) m)(\dot{\psi}_1 l_1 - 2\dot{\psi}_1 l_4 + 2\beta v_x - \delta_F v_x) \\
& + J m (3\dot{\psi}_1 \dot{v}_x (l_1 - l_4) + (3\beta - 2\delta_F) \dot{v}_x v_x + (\dot{\delta}_F + \dot{\psi}_1) v_x^2)) \Big)
\end{aligned} \tag{44}$$

2.3.3 Distance Between the Host Vehicle Path and the Lane

Assume a small arc du of the circumference describing the host vehicle's curvature, see Figure 4. The angle between the host vehicle and the road is δ_R, thus

$$dl_3 = du \sin \delta_R, \tag{45a}$$
$$\dot{l}_3 = v_x \sin \delta_R. \tag{45b}$$

2.4 Leading Vehicles

2.4.1 Geometric Constraints

The leading vehicles are also referred to as targets Tn. The coordinate frame L_{Tn} moving with target n is located in P_{Tn}, as we saw in Figure 3. It is assumed that the leading vehicles are driving on the road. More specifically, it is assumed that they are following the road curvature and thus that their heading is the same as the tangent of the road.

For each target Tn, there exists a coordinate frame L_{Sn}, with its origin P_{Sn} at the position of the sensor. Hence, the origin is the same for all targets, but the coordinate frames have different angles ψ_{Sn}. This angle, as well as the distance l_{Sn}, depend on the targets position in space. From Figure 3 it is clear that,

$$r^R_{P_4O} + r^R_{P_{Sn}P_4} + r^R_{P_{Tn}P_{Sn}} - r^R_{P_{Tn}O} = 0, \tag{46}$$

or split in x and y components:

$$x^R_{P_4O} + (l_2 - l_4)\cos\psi_1 + l_{Sn}\cos\psi_{Sn} - x^R_{P_{Tn}O} = 0, \tag{47a}$$
$$y^R_{P_4O} + (l_2 - l_4)\sin\psi_1 + l_{Sn}\sin\psi_{Sn} - y^R_{P_{Tn}O} = 0. \tag{47b}$$

Let us now define the relative angle to the leading vehicle as

$$\delta_{Sn} \triangleq \psi_{Sn} - \psi_1. \tag{48}$$

The road shape was described by (36) in the road frame L_3, where the x-axis is in the longitudinal direction of the vehicle. Differentiating (36) w.r.t. x^{L_3} results in

$$\frac{dy^{L_3}}{dx^{L_3}} = c_0 x^{L_3} + \frac{c_1 \left(x^{L_3}\right)^2}{2}. \tag{49}$$

The Cartesian x-coordinate of the leading vehicle P_{Tn} in the L_3-frame is:

$$x^{L_3}_{P_{Tn}P_3} = x^{L_1}_{P_{Tn}P_1} - l_2 = l_{Sn}\frac{\cos\delta_{Sn}}{\cos\delta_r}. \tag{50}$$

This gives us the angle of the leading vehicle relative to the road at P_3,

$$\delta_{Tn} = \psi_{Tn} - \psi_3 = \arctan\frac{dy^{L_3}}{dx^{L_3}} \qquad \text{for } x^{L_3} = x^{L_3}_{P_{Tn}P_3}, \tag{51}$$

which is not absolutely correct, since the leading vehicle must not drive directly on the road line. However, it is sufficient for our purposes.

2.4.2 Kinematic Constraints

The target Tn is assumed to have zero lateral velocity, i.e.,$\dot{y}^{L_{Sn}} = 0$. Furthermore, using the geometry of Figure 1 we have

$$A^{L_{Sn}R} \cdot \dot{r}^R_{P_{Tn}O} = \begin{pmatrix} \cdot \\ 0 \end{pmatrix}, \tag{52}$$

which can be rewritten as:

$$-\dot{x}^R_{P_{Tn}O} \sin\psi_{Sn} + \dot{y}^R_{P_{Tn}O} \cos\psi_{Sn} = 0. \tag{53}$$

2.4.3 Angle

The host vehicles velocity vector is applied in its CoG P_4. The derivative of (47) is used together with (16) and (53) to get an expression for the derivative of the relative angle to the leading vehicle w.r.t. time

$$(\dot{\delta}_{Sn} + \dot{\psi}_1) l_{Sn} + \dot{\psi}_1 (l_2 - l_4) \cos\delta_{Sn} + v_x \sin(\beta - \delta_{Sn}) = 0 \tag{54}$$

which is rewritten according to

$$\dot{\delta}_{Sn} = -\frac{\dot{\psi}_1 (l_2 - l_4) \cos\delta_{Sn} + v_x \sin(\beta - \delta_{Sn})}{l_{Sn}} - \dot{\psi}_1. \tag{55}$$

3 Resulting Sensor Fusion Problem

The resulting state-space model is divided into three parts, one for the host vehicle, one for the road and one for the leading vehicles, referred to as H, R and T, respectively. In the final state-space model the three parts are augmented, resulting in a state vector of dimension $6 + 4 \cdot$(Number of leading vehicles). Hence, the state vector varies with time, depending on the number of leading vehicles that we are currently tracking.

3.1 Dynamic Motion Model

We will in this section briefly summarize the dynamic motion models previously derived in Section 2. The host vehicle model is described by the following states,

$$x_H = \begin{pmatrix} \dot{\psi}_1 & \beta & l_3 \end{pmatrix}^T, \tag{56}$$

i.e., the yaw rate, the float angle and the distance to the left lane marking. The nonlinear states space model $\dot{x}_H = f_H(x, u)$ is given by

$$f_H(x,u) = \begin{pmatrix} \beta \frac{(-(l_1-l_4)C_{\alpha f}\cos\delta_F + l_4 C_{\alpha r})}{J} - \dot{\psi}_1 \frac{C_{\alpha f}(l_1-l_4)^2 \cos\delta_F + C_{\alpha r} l_4^2}{J v_x} + \frac{(l_1-l_4)C_{\alpha f}\tan\delta_F}{J} \\ \beta \frac{-C_{\alpha f}\cos\delta_F - C_{\alpha r} - \dot{v}_x m}{m v_x} - \dot{\psi}_1 \left(1 + \frac{C_{\alpha f}(l_1-l_4)\cos\delta_F - C_{\alpha r} l_4}{v_x^2 m}\right) + \frac{C_{\alpha f}\sin\delta_F}{m v_x} \\ v_x \sin\delta_R \end{pmatrix} \tag{57}$$

The corresponding differential equations were given in (29), (30) and (45b), respectively.

The states describing the road x_R are the road curvature at the host vehicle position c_0, the angle between the host vehicles direction of motion and the road curvature tangent δ_R and the width of the road W, i.e.,

$$x_R = \begin{pmatrix} c_0 & \delta_R & W \end{pmatrix}^T. \tag{58}$$

The differential equations for c_0 and δ_R were given in (44) and (41), respectively. When it comes to the width of the current lane W, we simply make use of

$$\dot{W} = 0, \tag{59}$$

motivated by the fact that W does not change as fast as the other variables, i.e. the nonlinear states space model $\dot{x}_R = f_R(x, u)$ is given by

$$f_R(x,u) = \begin{pmatrix} \dot{c}_0 \\ c_0 v_x - \beta \frac{-C_{\alpha f}\cos\delta_F - C_{\alpha r} - \dot{v}_x m}{m v_x} + \dot{\psi} \frac{C_{\alpha f}(l_1 - l_4)\cos\delta_F - C_{\alpha r} l_4}{v_x^2 m} - \frac{C_{\alpha f}\sin\delta_F}{m v_x} \\ 0 \end{pmatrix} \tag{60}$$

The states defining the targets are the azimuth angle δ_{S_n}, the lateral position l_{Tn} of the target, the distance between the target and the host vehicle l_{Sn} and the relative velocity between the target and the host vehicle $\dot{l}_{Sn}$. This gives the following state vector for a leading vehicle

$$x_T = \begin{pmatrix} \delta_{Sn} & l_{Tn} & \dot{l}_{Sn} & l_{Sn} \end{pmatrix}^T. \tag{61}$$

The derivative of the azimuth angle was given in (55). It is assumed that the leading vehicles lateral velocity is small, implying that $\dot{l}_{Tn} = 0$ is a good assumption (compare with Figure 3). Furthermore, it can be assumed that the leading vehicle accelerates similar to the host vehicle, thus $\ddot{l}_{Sn} = 0$ (compare with e.g., [6]). The states space model $\dot{x}_T = f_T(x, u)$ of the targets (leading vehicles) is

$$f_T(x,u) = \begin{pmatrix} -\frac{\dot{\psi}_1(l_2 - l_4)\cos\delta_{Sn} + v_x \sin(\beta - \delta_{Sn})}{l_{Sn}} - \dot{\psi}_1 \\ 0 \\ 0 \\ \dot{l}_{Sn} \end{pmatrix} \tag{62}$$

Furthermore, the steering wheel angle δ_F and the host vehicle longitudinal velocity v_x are modelled as input signals,

$$u_t = \begin{pmatrix} \delta_F & v_x \end{pmatrix}^T. \tag{63}$$

3.2 Measurement Equations

The measurement equation describes how the state variables relate to the measurements, i.e., it describes how the measurements enters the estimator. Recall that subscript m is used to denote measurements. Let us start by introducing the measurements relating directly to the host vehicle motion, by defining

$$y_1 = \begin{pmatrix} \dot{\Psi} & a_{y,m}^{L_4} \end{pmatrix}^T, \tag{64}$$

where $\dot{\Psi}$ and $a_{y,m}^{L_4}$ are the measured yaw rate and the measured lateral acceleration, respectively. They are both measured with the host vehicles inertial sensor in the center of gravity. In order to find the corresponding measurement equation we start by observing that the host vehicle's lateral acceleration in the CoG is

$$a_y^{L_4} = v_x(\dot{\psi} + \dot{\beta}) + \dot{v}_x\beta. \tag{65}$$

Combining this expression with the centrifugal force and assuming $\dot{v}_x\beta = 0$ yields

$$\begin{aligned} a_y^{L_4} = v_x(\dot{\psi} + \dot{\beta}) = \beta\frac{-C_{\alpha f} - C_{\alpha r} - m\dot{v}_x}{m} \\ + \dot{\psi}_1\frac{-C_{\alpha f}(l_1 - l_4) + C_{\alpha r}l_4}{mv_x} + \frac{C_{\alpha f}}{m}\delta_F \end{aligned} \tag{66}$$

From this equation it is clear that the sensor information from the host vehicle's inertial sensor, the yaw rate and the lateral acceleration, and the steering wheel angel contains information about the float angle β. Hence the measurement equations corresponding to (64) are given by

$$h_1 = \begin{pmatrix} \dot{\psi}_1 \\ \beta\frac{-C_{\alpha f}-C_{\alpha r}-m\dot{v}_x}{m} + \dot{\psi}_1\frac{-C_{\alpha f}(l_1-l_4)+C_{\alpha r}l_4}{mv_x} + \frac{C_{\alpha f}}{m}\delta_F \end{pmatrix} \tag{67}$$

The vision system provides measurements of the road geometry and the host vehicle position on the road according to

$$y_2 = \begin{pmatrix} c_{0,m} & \delta_{r,m} & W_m & l_{3,m} \end{pmatrix}^T \tag{68}$$

and the corresponding measurement equations are given by

$$h_2 = \begin{pmatrix} c_0 & (\delta_R + \beta) & W & l_3 \end{pmatrix}^T. \tag{69}$$

In order to include measurements of a leading vehicle we require that it is seen both by the radar and the vision system. The corresponding measurement vector is

$$y_3 = \begin{pmatrix} \delta_{Sn,m} & \dot{l}_{Sn,m} & l_{Sn,m} \end{pmatrix}^T. \tag{70}$$

Since these are state variables the measurement equation is obviously

$$h_3 = \begin{pmatrix} \delta_{Sn} & \dot{l}_{Sn} & l_{Sn} \end{pmatrix}^T. \tag{71}$$

Finally, we have to introduce a nontrivial artificial measurement equation in order to reduce the drift in l_{Tn}, and to introduce a further constraint on the road curvature. The measurement equation, which is derived from Figure 3 is given by

$$h_4 = \frac{c_0(l_{Sn}\cos\delta_{Sn})^2}{2} + \frac{l_{Tn}}{\cos\delta_{Tn}} + l_3 + l_{Sn}(\delta_R + \beta)\cos\delta_{Sn}, \tag{72}$$

and the corresponding measurement is simply

$$y_4 = l_{Sn,m}\sin(\delta_{Sn,m}). \tag{73}$$

This might seem a bit ad hoc at first. However, the validity of the approach has recently been justified in the literature, see e.g., [20].

3.3 Estimator

The state-space model derived in the previous section is nonlinear and it is given in continuous time, whereas the measurements are in discrete time. The filtered estimates $\hat{x}_{t|t}$ are computed with an EKF. In order to do this we will first linearize and discretize the state-space model. This is a standard situation and a solid account of the underlying theory concerning this can be found in e.g., [11, 18].

The discretization is performed using the standard forward Euler method, resulting in

$$x_{t+T} = x_t + Tf(x_t, u_t) = g(x_t, u_t) \tag{74}$$

where T denotes the sample time. Now, at each time step the nonlinear state-space model is linearized by evaluating the Jacobian (i.e., the partial derivatives) of the $g(x, u)$-matrix at the current estimate $\hat{x}_{t|t}$. It is worth noting that this Jacobian is straightforwardly computed off-line using symbolic software, such as MATHEMATICA.

The leading vehicles are estimated using rather standard techniques from target tracking, such as nearest neighbour data association and track counters in order to decide when to stop tracking a certain vehicle, etc. These are all important parts of the system we have implemented. However, it falls outside the scope of this paper and since the techniques are rather standard we reference the general treatments given in e.g., [2, 1].

4 Experiments and Results

The experiments presented in this section are based on measurements acquired on public roads in Sweden during normal traffic circumstances. The host vehicle was equipped with radar and vision systems, measuring the distances and angles to the leading vehicles (targets). Information about the host vehicle motion, such as the steering wheel angle, yaw rate, etc. where acquired directly from the CAN bus.

4.1 Parameter Estimation

Most of the host vehicle's parameters, such as the dimensions, the mass and the moment of inertia, were given by the vehicle manufacturer (OEM). Since the cornering stiffness is a parameter which describes the properties between road and tire it has to be estimated for the given set of measurements.

4.1.1 Cornering Stiffness Parameters

A state space model with the states,

$$x = \begin{pmatrix} \dot{\psi} & \beta \end{pmatrix}^T, \tag{75}$$

i.e., the yaw rate and the float angle and the differential equations in (29) and (30) was used. Furthermore, the steering wheel angle and the host vehicle longitudinal velocity were modeled as input signals

$$u = \begin{pmatrix} \delta_F & v_x \end{pmatrix}^T. \tag{76}$$

The yaw rate and the lateral acceleration

$$y = \begin{pmatrix} \dot{\psi} & a_y \end{pmatrix}^T, \tag{77}$$

were used as outputs of the state space model and the measurement equation was given in (67).

For this rather straightforward method we used two `for`-loops iterating the state space model with the estimation data for cornering stiffness values between 50,000 and 100,000 N/rad. The estimated yaw rate and lateral acceleration was compared with the measured values using the best fit value defined by

$$\text{fit} = \left(1 - \frac{|y - \hat{y}|}{|y - \bar{y}|}\right) \cdot 100 \tag{78}$$

where y is the measured value, $\hat{y}$ is the estimate and $\bar{y}$ is the mean of the measurement. The two fit-values where combined in a weighted sum forming a joint fit-value. In Figure 6 a diagonal ridge of the best fit value is clearly identifiable. For different estimation data sets, different local maxima were found on the ridge. However, it feels natural to assume that the two parameters should have approximately the same value. This constraint (which forms a cross diagonal or orthogonal ridge) is expressed as

$$\text{fit}_{\text{para}} = \left(1 - \frac{|C_{\alpha f} - C_{\alpha r}|}{\left|\frac{(C_{\alpha f} + C_{\alpha r})}{2}\right|}\right) \cdot 100. \tag{79}$$

and added as a third fit-value to the weighted sum, obtaining the total best fit for the estimation data set as

$$\text{best total fit} = \text{W}_{\psi}\text{fit}_{\psi} + \text{W}_{a_y}\text{fit}_{a_y} + \text{W}_{\text{para}}\text{fit}_{\text{para}}, \tag{80}$$

where

$$\text{W}_{\psi} + \text{W}_{a_y} + \text{W}_{\text{para}} = 1 \tag{81}$$

The iteration resulted in the values $C_{\alpha f} = 69,000$ N/rad and $C_{\alpha r} = 81,000$ N/rad.

The state space model was validated with the given parameters, see Figure 7. The fit-values of the yaw rate and lateral acceleration are given together with some standard liner and nonlinear system identification approaches in Table 1.

4.1.2 Kalman Design Variables

The process and measurement noise covariances (Q and R matrices) are design parameters of the extended Kalman filter (EKF). It is assumed that there are no cross correlations between the measurement signals or the process equations, i.e. the two matrices are diagonal. The present filter has ten states and ten measurement signals, which implies that 20 parameters have to be tuned. The tuning was started by using physical intuition of the error of the process equation and the measurement signals. In a second step the covariance parameters were tuned by an algorithm minimizing the root mean square error (RMSE) of the estimated $\hat{c}_0$ and the reference curvature c_0. The estimated curvature was

Table 1: Fit values for some different identification approaches. The Grid approach was discussed in this section, the tree others are nonlinear and linear methods available in MATLAB'S SYSTEM IDENTIFICATION TOOLBOX. Note that the two last linear black-box approaches have no explicit cornering stiffness parameters. The fit values are presented for the two outputs, the yaw rate and the lateral acceleration respectively.

Approach	Fit Yaw Rate [%]	Fit Latt. Acc. [%]
Grid	66	71
NL-Gray	57	56
ARX	75	67
Subspace	69	65

obtained by simulating the filter with an estimation data set. The calculation of the reference value is described in [7].

The tuning algorithm adjusts the elements of the diagonal Q and R matrices sequentially, i.e. tuning the first element until the minimum RMSE value is found, thereafter tuning the next element and so on. When all elements have been adjusted the algorithm starts with the first again. This procedure is iterated until the RMSE value is stabilized, and a local minima has been found:

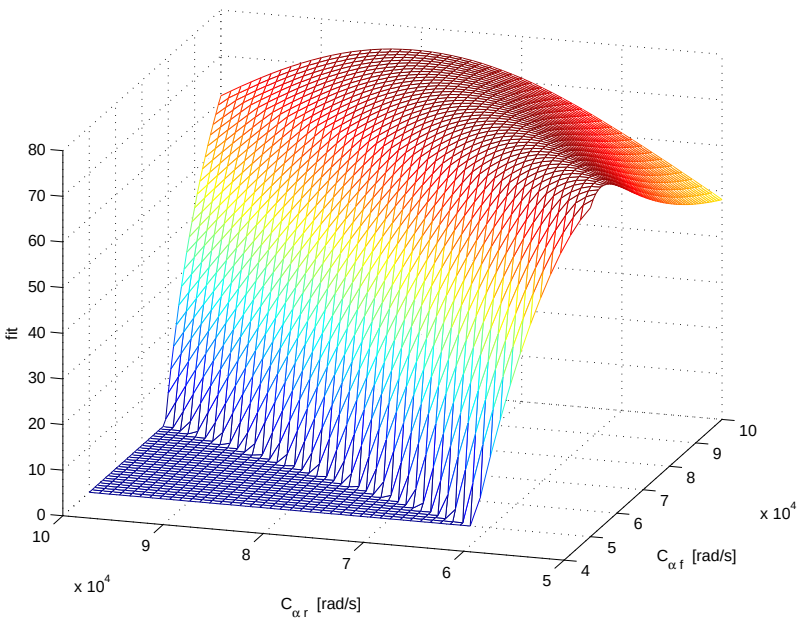

Figure 6: Total best fit value of the two outputs and the constraint defined in (79).

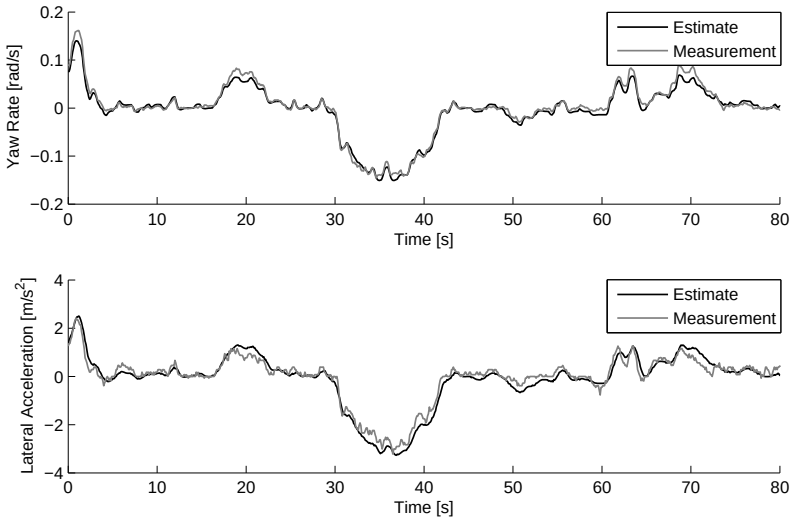

Figure 7: Comparing the simulated result of the nonlinear state space model (black) with measured data (gray) of a validation data set. The upper plot shows the yaw rate and the lower shows the lateral acceleration.

1. Start with initial values of the parameter $p(n)$, where $n = 1...20$ for the present filter. Simulate the filter and save the resulting RMSE value in the variable `old RMSE`.

2. Simulate the filter for three different choices of the parameter $p(n)$:

   - $p(n)(1 + \Delta)$
   - $p(n)(1 - \Delta)$.
   - $p(n)(1 + \delta)$ with $\delta = \mathcal{N}(0, 0.1)$.

3. Assign $p(n)$ the value corresponding to smallest RMSE of these three choices or the old value of $p(n)$. Save the RMSE in the variable `current RMSE`. If the value of $p(n)$ was changed go to 2, if it was not changed and if $n \neq n_{max}$ switch parameter `n:=n+1` and go to 2.

4. Compare the current with old RMSE value, if there is no difference stop. Use the difference between the current and the old RMSE to calculate Δ (limit the value to e.g $0.001 < \Delta < 0.1$). Assign `old RMSE := current RMSE` and go to 2.

The chosen design parameters were validated on a different data set, the results are discussed in the next sections.

4.2 Validation of Host Vehicle Signals

The host vehicle's states are according to (56), the yaw rate, the float angle and the distance to the left lane marking. The estimated and the measured yaw rate signals are as expected very similar. As described in Section 4.1.1, the

parameters of the vehicle model were optimized with respect to the yaw rate, hence it is no surprise that the fusion method decrease the residual further. A sequence from a measurement on a rural road is shown in Figure 8. Note that the same measurement sequence is used in the Figures 7 to 13, which will make it easier to compare the estimated states.

The float angle β is estimated, but there exists no reference or measurement signal. An example is shown in Figure 9. For velocities above 30-40 km/h, the float angle appears more or less like the mirror image of the yaw rate, and by comparing with Figures 8 we can conclude that the sequence is consistent.

The measurement signal of the distance to the left white lane marking $l_{3,m}$ is produced by the vision system OLR (Optical Lane Recognition). Bad lane

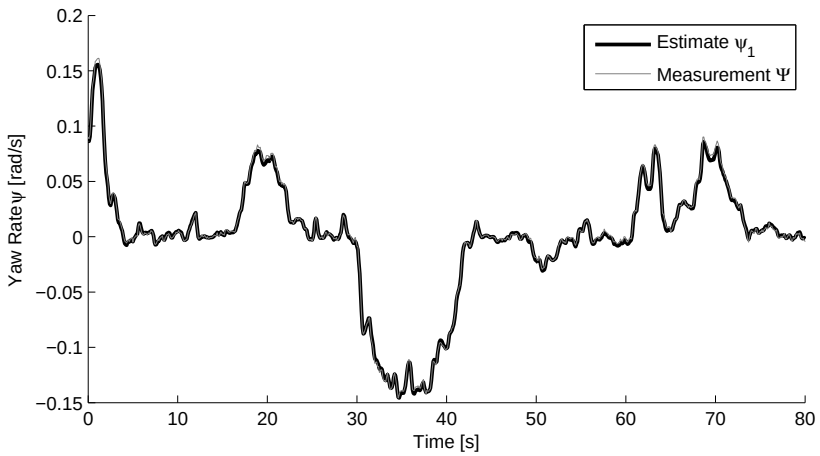

Figure 8: Comparison between the measured (gray) and estimated yaw rate using the sensor fusion approach in this paper (black).

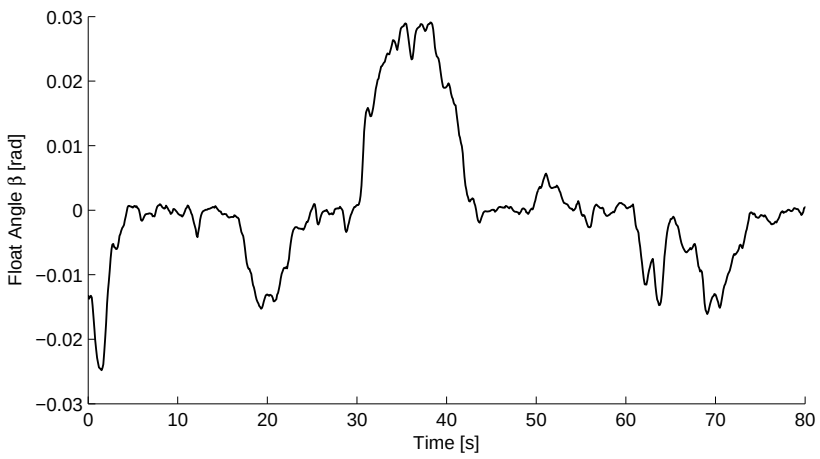

Figure 9: The estimated float angle β for the same measurement as used for the yaw rate in Figure 8.

markings or certain weather conditions can cause errors or noise in the measurement signal. The estimated state l_3 of the fusion approach is very similar to the pure OLR signal as shown in Figure 10.

The measured and estimated angle between the host vehicles direction of motion (velocity vector) and the road curvature tangent δ_R is shown in Figure 11. The measurement signal is produced by the OLR.

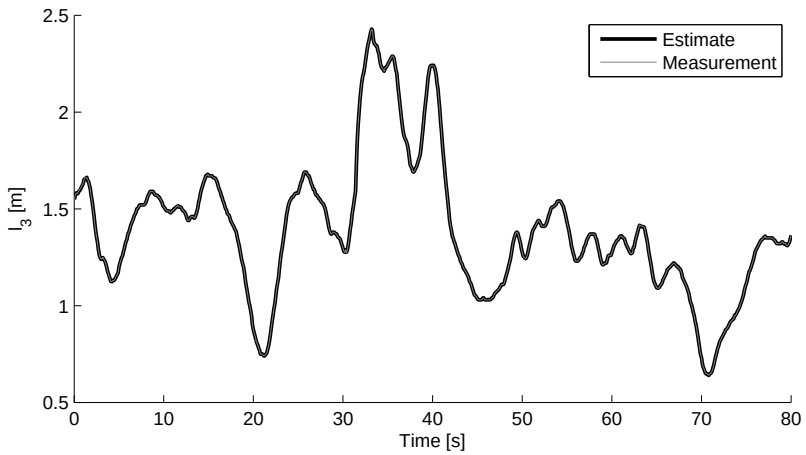

Figure 10: The estimated and measured distance to the left white lane marking l_3.

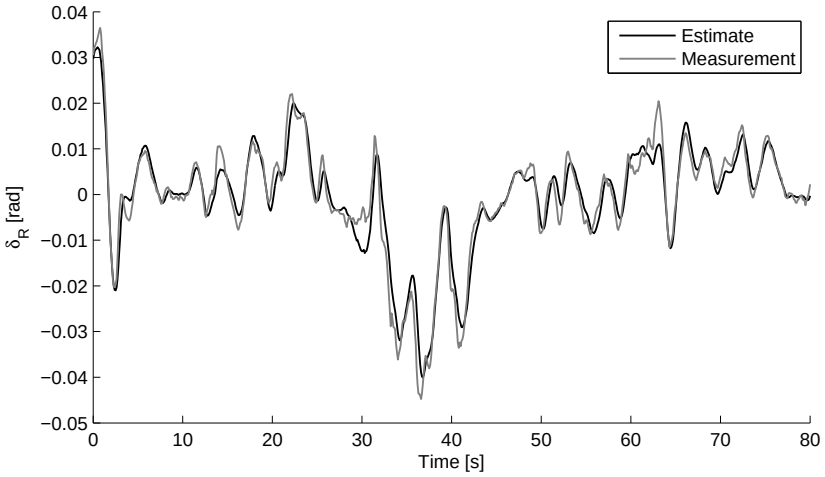

Figure 11: The estimated and measured angle between the velocity vector of the host vehicle and the tangent of the road δ_R.

4.3 Road Curvature Estimation

An essential idea with the sensor fusion approach shown in this paper is to make use of a more precise host vehicle model in order to estimate the road curvature. In this section we will compare this approach with other vehicle and road models. There are basically two differences in comparison with other fusion approaches discussed in the literature,

1. the more precise host vehicle model including the float angle β and
2. the dynamic curvature model (44).

We will compare three fusion approaches and two more straightforward approaches.

Fusion 1 is the sensor fusion approach shown in this paper.

Fusion 2 is a similar approach, thoroughly described in [6]. An important difference to fusion 1 is that the host vehicle model is less complex and the float angle β among others is not modeled. Furthermore, in fusion 2, the road is modeled according to (38) and a road aligned coordinate frame is used.

Fusion 3 comprehends the host vehicle model of fusion 1 and the road model of fusion 2, i.e. substituting (44) by (38) and introducing the seventh state c_1. This method is described in e.g. [4].

Model 1 estimates the curvature as a division of two measurement signals

$$\hat{c}_0 = \frac{\Psi}{v_x} \tag{82}$$

i.e. the model comprises no dynamics.

Model 2 is the state space model described in Section 3.3, i.e. the model of this paper is used as estimator without the Kalman filter.

Before we analyze the results we discuss the important question of where the curvature coefficient c_0 is defined. In fusion 1 and the two models it feels rather natural to assume that c_0 is defined at the host vehicle and thus describes the currently driven curvature. In fusion 2 and 3 the curvature is described by the state space model (38) and by the polynomials (34) and (36) respectively, both utilizing two curvature coefficients c_0 and c_1. In this case it is more difficult to define of the position of c_0 by intuition.

The curvature estimate $\hat{c}_0$ from the sensor fusion approaches are compared to the estimate from the optical lane recognition (OLR) alone and a reference value (computed off-line using [7]). A typical result of this is shown in Figure 12. The data stems from a rural road, which explains the curvature values. It can be seen that the estimates from the sensor fusion approaches gives better results than using the OLR alone, as was expected. The OLR estimate is rather noisy compared to the fused estimates. This is not surprising, since the pure OLR has less information.

Fusion 3, model 1 and model 2 are shown together with the reference value in Figure 13. The curvature estimate from model 1 (gray solid line) is surprisingly

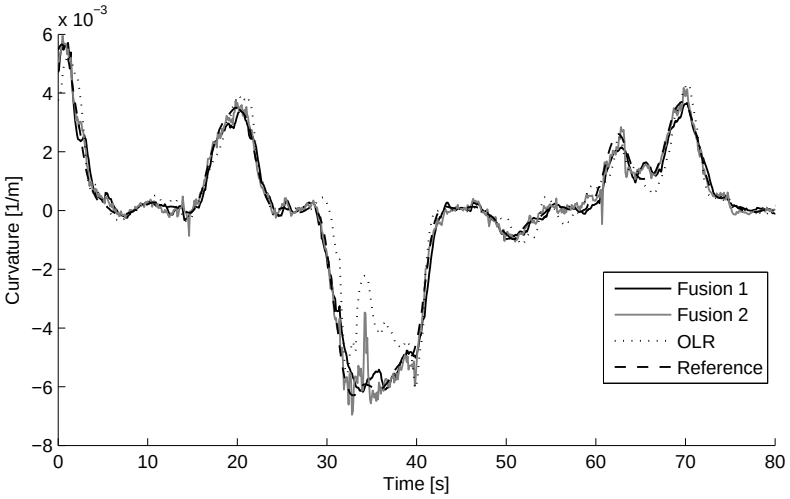

Figure 12: Results from the two fusion approaches (fusion 1 solid black line and fusion 2 gray line) and the OLR (dotted line), showing the curvature estimate $\hat{c}_0$. As can be seen the curvature estimation can be improved by taking the other vehicles (gray line) and the host vehicle's driven curvature in account (solid black line). The dashed line is the reference curvature.

good, considering the fact that it is just a division of two measurement signals. Model 2 (solid black line) is the state space model described in this paper. The absolute position is not measured and the derivative of the curvature is estimated, which leads to a major bias on the estimate of c_0. The bias is transparent in Figure 13 but it also leads to a large RMSE value in Table 2. Fusion 3 also gives a proper result, it is interesting to notice that the estimate seams to follow the incorrect OLR at 35 s. The same behavior holds for fusion 2 in Figure 12, which uses the same road model.

To get a more aggregate view of the performance, we give the root mean square error (RMSE) for longer measurement sequences in Table 2. The fusion approaches improves the road curvature estimate by making use of the information about the leading vehicles, that is available from the radar and the vision systems. However, since we are interested in the curvature estimate also when there are no leading vehicles in front of the host vehicle this case will be studied as well. It is straightforward to study this case, it is just a matter of not providing the measurements of the leading vehicles to the algorithms. In Table 2 the RMSE values are provided for a few different scenarios. It is interesting to see that the advantage of fusion 1, which uses a more accurate host vehicle model, in comparison to fusion 2 is particularly noticeable when driving alone on a rural road. The reason for this is first of all that there are no leading vehicles that could aid the fusion algorithm. Furthermore, the fact that we are driving on a rather curvy road implies that any additional information will help improving the curvature estimate. Here, the additional information is the improved host vehicle model used in fusion 1. The highway is rather straight and as expected not much accuracy could be gained in using an improved dynamic vehicle model.

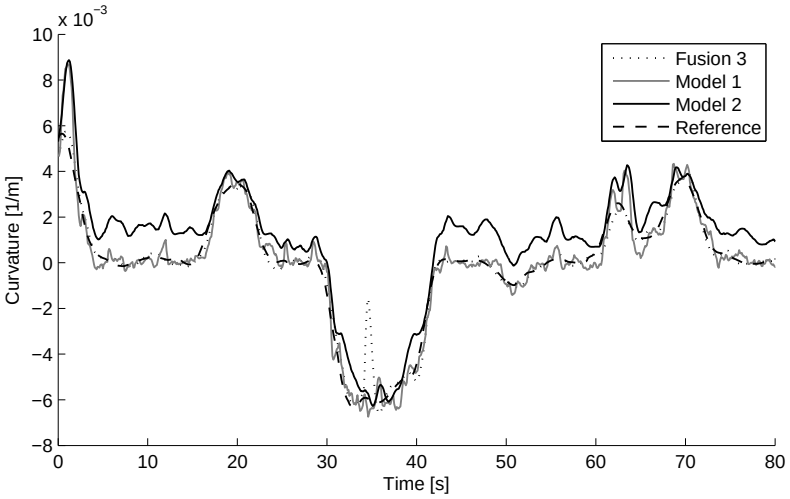

Figure 13: Results from fusion 3 (dotted line) and the two models (model 1 gray line and model 2 solid black line), showing the curvature estimate $\hat{c}_0$. Model 2 is estimating the derivative of the curvature and the absolute position is not measured, which leads to the illustrated bias. The dashed line is the reference curvature.

4.4 Leading Vehicle Tracking

A common problem with these road estimation methods is that it is hard to distinguish between the case when the leading vehicle is entering a curve and the case when the leading vehicle is performing a lane change. With the approach in this paper the information about the host vehicle motion, the OLR and the leading vehicles is weighted together in order to form an estimate of the road curvature. Figure 14 shows an example from a situation on a three lane highway, where one of the leading vehicles changes lane. The fusion approach

Table 2: Comparison of the root mean square error (RMSE) values for the three fusion approaches and the pure measurement signal OLR for two longer measurement sequence on public roads. Two cases where considered, using the knowledge of the leading vehicles position or not and thereby simulating the lonely driver. Note that all RMSE values should be multiplied by 10^{-3}.

$\cdot 10^{-3}$	Highway		Rural road	
Time	15 min		9 min	
OLR	0.152		0.541	
Model 1	0.193		0.399	
Model 2	0.311		1.103	
Leading vehicles used?	yes	no	yes	no
Fusion 1 (this paper)	0.103	0.138	0.260	0.387
Fusion 2 (method from [6])	0.126	0.143	0.266	0.499
Fusion 3	0.154	0.152	0.331	0.403

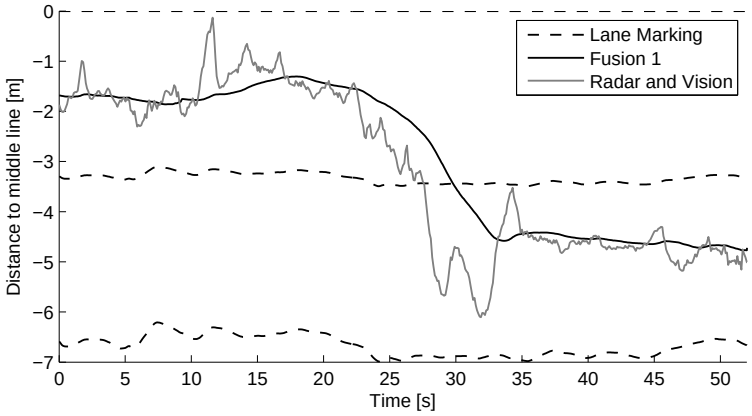

Figure 14: Illustration of the lateral movement l_{Tn} over time for a leading vehicle driving on a highway with three lanes, where the leading vehicle changes lane. The estimate from our fusion approach (fusion 1) is given by the solid black lines and the raw measurement signal is shown by the solid gray line. The dashed lines shows the lane markings. In this example the distance to the leading vehicle is 65 m, see Figure 15.

in this paper produces an estimate of the lateral position of the leading vehicle which seems reasonable, but there is a time delay present in the estimate. To get a better understanding of this situation, one of the images acquired during the lane change is shown in Figure 15.

For straight roads with several leading vehicles no difference between this and the second fusion approach mentioned above could be seen. This can be explained by the other leading vehicles, which stay in there lane and stabilizes the road geometry estimation.

Figure 15: Camera view for the situation in Figure 14 during the lane change. The distance to the leading vehicle is approximately 65 m.

5 Conclusions

We have presented a new formulation for the well studied problem of integrated road geometry estimation and vehicle tracking. The main differences to the existing approaches are that we have introduced a new dynamic model for the road and we make use of an improved host vehicle model. The results obtained using measurements from real traffic situations clearly indicates that the gain in using the extended host vehicle model is most prominent when driving on rural roads without any vehicles in front.

6 Acknowledgement

The authors would like to thank Dr. Andreas Eidehall at Volvo Car Corporation for fruitful discussions. Furthermore, they would like to thank the SEnsor Fusion for Safety (SEFS) project within the Intelligent Vehicle Safety Systems (IVSS) program for financial support.

References

[1] Y. Bar-Shalom, X. R. Li, and T. Kirubarajan. *Estimation with Applications to Tracking and Navigation*. John Wiley & Sons, New York, 2001.

[2] S. S. Blackman and R. Popoli. *Design and Analysis of Modern Tracking Systems*. Artech House, Inc., Norwood, MA, USA, 1999.

[3] E. D. Dickmanns. *Dynamic Vision for Perception and Control of Motion*. Springer, 2007.

[4] E. D. Dickmanns and B. D. Mysliwetz. Recursive 3-D road and relative ego-state recognition. *IEEE Transactions on pattern analysis and machine intelligence*, 14(2):199–213, February 1992.

[5] E. D. Dickmanns and A. Zapp. A curvature-based scheme for improving road vehicle guidance by computer vision. In *Proceedings of the SPIE Conference on Mobile Robots*, volume 727, pages 161–198, Cambridge, MA, USA, 1986.

[6] A. Eidehall. *Tracking and threat assessment for automotive collision avoidance*. Phd thesis No 2007, Linköping Studies in Science and Technology, SE-581 83 Linköping, Sweden, January 2007.

[7] A. Eidehall and F. Gustafsson. Obtaining reference road geometry parameters from recorded sensor data. In *Proceedings of the IEEE Intelligent Vehicles Symposium*, pages 256–260, Tokyo, Japan, June 2006.

[8] A. Eidehall, J. Pohl, and F. Gustafsson. Joint road geometry estimation and vehicle tracking. *Control Engineering Practice*, 15(12):1484–1494, December 2007.

[9] A. Gern, U. Franke, and P. Levi. Advanced lane recognition - fusing vision and radar. In *Proceedings of the IEEE Intelligent Vehicles Symposimum*, pages 45–51, Dearborn, MI, USA, October 2000.

[10] A. Gern, U. Franke, and P. Levi. Robust vehicle tracking fusing radar and vision. In *Proceedings of the international conference of multisensor fusion and integration for intelligent systems*, pages 323–328, Baden-Baden, Germany, August 2001.

[11] F. Gustafsson. *Adaptive Filtering and Change Detection*. John Wiley & Sons, New York, USA, 2000.

[12] H. Hahn. *Rigid body dynamics of mechanisms. 1, Theoretical basis*, volume 1. Springer, Berlin, Germany, 2002.

[13] T. Kailath, A. H. Sayed, and B. Hassibi. *Linear Estimation*. Information and System Sciences Series. Prentice Hall, Upper Saddle River, NJ, USA, 2000.

[14] U. Kiencke and L. Nielsen. *Automotive Control Systems*. Springer, Berlin, Heidelberg, Germany, second edition, 2005.

[15] B.B. Litkouhi, A.Y. Lee, and D.B. Craig. Estimator and controller design for lanetrak, a vision-based automatic vehicle steering system. In *Proceedings of the 32nd IEEE Conference on Decision and Control*, volume 2, pages 1868 – 1873, San Antonio, Texas, December 1993.

[16] M. Mitschke and H. Wallentowitz. *Dynamik der Kraftfahrzeuge*. Springer, Berlin, Heidelberg, 4th edition, 2004.

[17] Robert Bosch GmbH, editor. *Automotive Handbook*. SAE Society of Automotive Engineers, 6th edition, 2004.

[18] W. J. Rugh. *Linear System Theory*. Information and system sciences series. Prentice Hall, Upper Saddle River, NJ, USA, second edition, 1996.

[19] T. B. Schön, A. Eidehall, and F. Gustafsson. Lane departure detection for improved road geometry estimation. In *Proceedings of the IEEE Intelligent Vehicle Symposium*, pages 546–551, Tokyo, Japan, June 2006.

[20] B. O. S. Teixeira, J. Chandrasekar, L. A. B. Torres, L. A. Aguirre, and D. S. Bernstein. State estimation for equality-constrained linear systems. In *Proceedings of the 46th Conference on Decision and Control (CDC)*, pages 6220–6225, New Orleans, LA, USA, December 2007.

[21] Z. Zomotor and U. Franke. Sensor fusion for improved vision based lane recognition and object tracking with range-finders. In *Proceedings of IEEE Conference on Intelligent Transportation System*, pages 595–600, Boston, MA, USA, November 1997.

Avdelning, Institution
Division, Department

Division of Automatic Control
Department of Electrical Engineering

Datum
Date

2008-03-03

Språk
Language

☐ Svenska/Swedish
☒ Engelska/English
☐ _____

Rapporttyp
Report category

☐ Licentiatavhandling
☐ Examensarbete
☐ C-uppsats
☐ D-uppsats
☒ Övrig rapport
☐ _____

ISBN
—

ISRN
—

Serietitel och serienummer
Title of series, numbering

ISSN
1400-3902

LiTH-ISY-R-2844

URL för elektronisk version

http://www.control.isy.liu.se

Titel
Title

Road Geometry Estimation and Vehicle Tracking using a Single Track Model

Författare
Author

Christian Lundquist, Thomas B. Schön

Sammanfattning
Abstract

This paper is concerned with the, by now rather well studied, problem of integrated road geometry estimation and vehicle tracking. The main differences to the existing approaches are that we make use of an improved host vehicle model and a new dynamic model for the road. The problem is posed within a standard sensor fusion framework, allowing us to make good use of the available sensor information. The performance of the solution is evaluated using measurements from real and relevant traffic environments from public roads in Sweden.

Nyckelord
Keywords

road geometry, vehicle tracking, sensor fusion, Kalman filter, single track model